

Fast optical indicator created with multi-ring moiré patterns

Emin Gabrielyan

Switzernet Sàrl, Scientific Park of Swiss Federal
Institute of Technology, Lausanne (EPFL)
emin.gabrielyan@switzernet.com

ABSTRACT

In mechanical measurement devices where measured values are indicated with a mechanical pointer and a graduated scale, the observation precision is increased often by adding an auxiliary mechanical pointer with a sub graduated scale. The auxiliary pointer moves in synchronization with the main pointer but at a higher speed. A constant velocity ratio between the auxiliary pointer and the main pointer is maintained via cogwheel type gearboxes. Mechanical solutions are not always suitable. A challenging idea is to use moiré phenomenon for its well known magnification and acceleration properties. However the well known moiré shapes with sufficient sharpness, good luminosity and contrast can be obtained only in highly periodic patterns. The periodic nature of patterns makes them inapplicable for indication of values. We present new discrete patterns assembled from simple moiré patterns of different periodicity. The elevation profile of our discrete pattern reveals a joint moiré shape with an arbitrarily long period. The luminosity and the sharpness of our shapes are as high as in simple highly periodic moiré.

Keywords: moiré, instrumentation, metrology, multi-stripe moiré, multi-ring moiré, non-periodic moiré, optical speedup, moiré indicator, moiré pointer, moiré watches, optical clock-hands, moiré clock-hands

1. INTRODUCTION

A graduated scale and a mechanical pointer is a common part for almost all mechanical measurement devices. Often an auxiliary pointer and a scale with sub graduations are used for additional precisions. The auxiliary pointer moves faster, in synchronization with the main pointer. The pointers are connected via a tooth wheel type transmission system. The involute tooth shape is one that results in a constant velocity ratio, and is the most commonly used in instrumentation gearing, clocks and watches. Mechanical methods for changing the speed however can often be heavy and inapplicable. Lack of the force, such as in a compass, can be one of the serious obstacles. Inertia problems arising from discrete movements of mechanical parts at high speed, such as in chronographs, may be another obstacle.

The magnification and acceleration properties of moiré superposition images are a well known phenomenon. The superposition of transparent structures, comprising periodic opaque patterns, forms periodic moiré patterns. A challenging idea would be to use optical moiré effect for creating a fast auxiliary pointer replacing completely the mechanical parts moving at high speeds. The periodic nature of known moiré patterns make them inappropriate for indication of values. Profiles with very long periods can be created with periodic moiré. It is possible to design circular layer patterns with radial lines such that their superposition produces a radial moiré fringe with an angular period equal to 360 degrees. Thus only single radial moiré fringe will be visible in the superposition pattern. However such long periods make the moiré fringes blurred. The dispersion area of the fringe can be as large as the half of the period. In section 4 we show a particular case where a radial periodic moiré can be of use with an additional design extension. However in general, the long period moiré fringes of classical periodic moiré are too inexact for indication purposes.

A limited degree of sharpening of shapes in periodic moiré is possible using band moiré methods, namely moiré magnification of micro shapes [Hutley99], [Kamal98]. Such shapes however require serious sacrifices of the overall luminosity of the superposition image without significant improvements of the sharpness.

Random moiré, namely Glass patterns, produce non-periodic superposition patterns [Amidror03a], [Amidror03b], [Glass69a], [Glass73a]. The obstacle is that the valid range of movements of layers is very limited. The auxiliary indicator would show the sub graduations only within the range of only one graduation of the main scale. Additionally, in random moiré the shapes are noisier than in simple periodic moiré.

We developed new discrete patterns formed by merging straight stripes or circular rings of simple periodic moiré patterns. The composing stripes or rings are simple patterns with carefully chosen periods and phases. The composite pattern reveals a sharp moiré shape with an arbitrarily long periodicity. Movement of a layer along the stripes or along the circumferences of rings produces a faster movement of the moiré shape. Such shape has all qualities for playing the role of the fast auxiliary indicator. The one of the layers can be put into slow mechanical motion by the main pointer of the measurement device. In our discrete patterns the shapes are as sharp as in highly periodic moiré patterns. The period of the moiré pointer can be as long as it is required by the display size of the instrument. In our discrete patterns, the choice of the period has no impact on the quality of the optical shape and a wide range of speed ratios can be obtained.

Choice of stripes or rings depends on the type of the movement of layers. For linear movements the pattern comprises parallel stripes following the path of the movement. For circular movements the pattern consists of concentric rings with a center corresponding to the rotation axis. Our algorithm merges numerous simple periodic patterns into a composite pattern so as to form a continuous joint shape in the assembled superposition image. The underlying layer patterns do not join into continuous shapes within assembled layers. The composite patterns are constructed, such that the velocity ratios across all individual moiré patterns are identical. Consequently, the joint shape of the multi-stripe or multi-ring moiré pattern conserves its form during movements of the optical image. The speed ratio and the sharpness of moiré shape are constant within the full range of movements of the main pointer and layers.

Circular multi-ring samples are the most interesting. They can be used for adding auxiliary optical pointers to numerous measurement device with circular dials and radial mechanical pointers such as clocks, watches, chronographs, protractors, thermometers, altimeters, barometers, compasses, speedometers, alidades, and even weathervanes. In mechanical chronographs, optical acceleration permits measuring fractions of seconds without having mechanical parts moving at high speed with related problems of force, inertia, stress, and wear.

The paper is organized as follows. Section 2 introduces the classical periodic moiré and the methods for forming periodic moiré fringes of a desired shape. These methods are presented in scope of a new perspective for easily changing the curves of moiré shapes without affecting the periodicity and the velocity ratios, which are essential parameters for the metrology purposes. Linear movements are considered and a set of corresponding equations is introduced. Section 3 introduces the equations for creating curved moiré shapes for rotating layers preserving the angular periodicity and velocity ratio. Section 4 presents an application of classical moiré. In sections 4 and 5 we present multi-ring moiré with various curved layer patterns and moiré superposition patterns. The conclusions are presented in section 7.

2. SIMPLE MOIRÉ PATTERNS

2.1. Superposition of layers with periodically repeating parallel lines

Simple moiré patterns can be observed when superposing two transparent layers comprising periodically repeating opaque parallel lines as shown in Figure 1. In the example, the lines of one layer are parallel to the lines of the second layer. The superposition image outlines periodically repeating dark parallel bands, called moiré lines. Spacing between the moiré lines is much larger than the periodicity of lines in the layers.

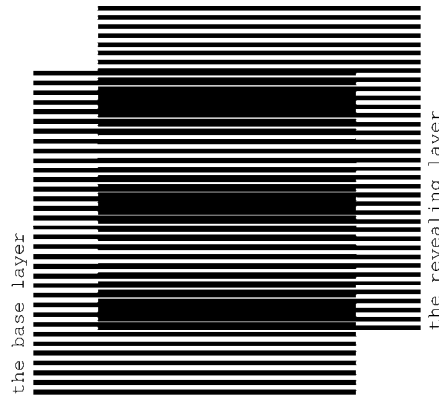


Figure 1. Superposition of two layers consisting of parallel lines, where the lines of the revealing layer are parallel to the lines of the base layer [\[eps\]](#), [\[tif\]](#), [\[png\]](#)

We denote one of the layers as the *base layer* and the other one as the *revealing layer*. When considering printed samples we assume that the revealing layer is printed on a transparency and is superposed on top of the base layer, which can be printed either on a transparency or on an opaque paper. The periods of the two layer patterns, i.e. the space between the axes of parallel lines, are close. We denote the period of the base layer as p_b and the period of the revealing layer as p_r . In Figure 1, the ratio p_b/p_r is equal to 12/11.

Light areas of the superposition image correspond to the zones where the lines of both layers overlap. The dark areas of the superposition image forming the moiré lines correspond to the zones where the lines of the two layers interleave, hiding the white background. Such superposition images are discussed in details in literature [\[Sciammarella62a p.584\]](#), [\[Gabrielyan07a\]](#).

The period p_m of moiré lines is the distance from one point where the lines of both layers overlap to the next such point. For cases represented by Figure 1 one can obtain the well known formula for the period p_m of the superposition image [\[Amidror00a p.20\]](#), [\[Gabrielyan07a\]](#):

$$p_m = \frac{p_b \cdot p_r}{p_b - p_r} \quad (2.1)$$

The superposition of two layers comprising parallel lines forms an optical image comprising parallel moiré lines with a magnified period. According to equation (2.1), the closer the periods of the two layers, the stronger the magnification factor is.

For the case when the revealing layer period is longer than the base layer period, the space between moiré lines of the superposition pattern is the absolute value of formula of (2.1).

The thicknesses of layer lines affect the overall darkness of the superposition image and the thickness of the moiré lines, but the period p_m does not depend on the layer lines' thickness. In our examples the base layer lines' thickness is equal to $p_b/2$, and the revealing layer lines' thickness is equal to $p_r/2$.

2.2. Speedup of movements with Moiré

If we slowly move the revealing layer of Figure 1 perpendicularly to layer lines, the moiré bands will start moving along the same axis at a several times faster speed. The four images of Figure 2 show the superposition image for different positions of the revealing layer. Compared with the first image (a) of Figure 2, in the second image (b) the revealing layer is shifted up by one fourth of the revealing layer period ($p_r \cdot 1/4$), in the third image (c) the revealing layer is shifted up by half of the revealing layer period ($p_r \cdot 2/4$), and in the fourth image (d) the revealing layer is shifted up by three fourth of the revealing layer period ($p_r \cdot 3/4$). The images show that the moiré lines of the superposition image move up at a speed, much faster than the speed of movement of the revealing layer.

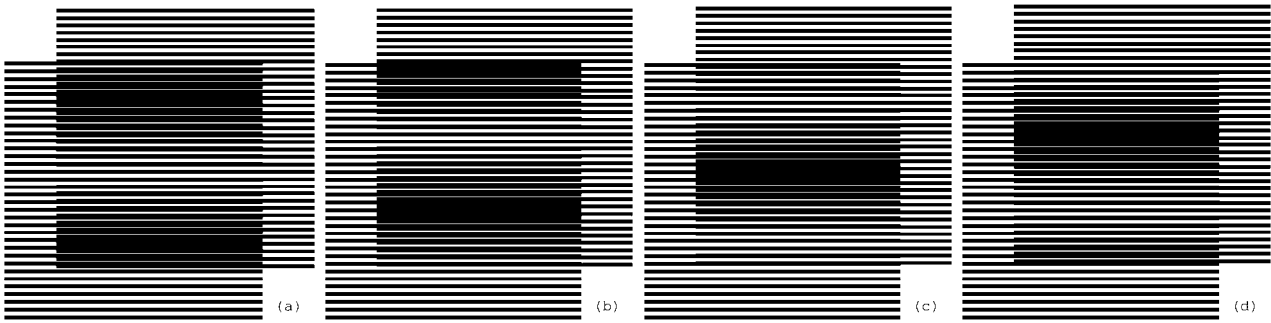


Figure 2. Superposition of two layers with parallel horizontal lines, where the revealing layer moves vertically at a slow speed [\[eps \(a\)\]](#), [\[png \(a\)\]](#), [\[eps \(b\)\]](#), [\[png \(b\)\]](#), [\[eps \(c\)\]](#), [\[png \(c\)\]](#), [\[eps \(d\)\]](#), [\[png \(d\)\]](#), GIF animation [\[ps\]](#), [\[gif\]](#), [\[tif\]](#)

When the revealing layer is shifted up perpendicularly to the layer lines by one full period (p_r) of its pattern, the superposition optical image must be the same as the initial one. It means that the moiré lines traverse a distance equal to the period of the superposition image p_m , while the revealing layer traverses the distance equal to its period p_r . Assuming that the base layer is immobile ($v_b = 0$), the following equation holds for the ratio of the optical image's speed to the revealing layer's speed:

$$\frac{v_m}{v_r} = \frac{p_m}{p_r} \quad (2.2)$$

According to equation (2.1) we have:

$$\frac{v_m}{v_r} = \frac{p_b}{p_b - p_r} \quad (2.3)$$

In case the period of the revealing layer is longer than the period of the base layer, the optical image moves in the opposite direction. The negative value of the ratio computed according to equation (2.3) signifies the movement in the reverse direction.

The GIF animation [\[gif\]](#) of the superposition image of Figure 1 showing a slow movement of the revealing layer is available on our web page [\[Gabrielyan07b\]](#).

2.3. Superposition of layers with inclined lines

In this section we introduce equations for patterns with inclined lines. Equations for rotated patterns were already introduced decades ago [Nishijima64a], [Oster63a], [Morse61a]. These equations are good for static moiré patterns or their static instances. In scope of metrology instrumentation, we review the equations suiting them for dynamic properties of moiré patterns. The set of key parameters is defined and the equations are developed such that the curves can be constructed or modified without affecting given dynamic properties.

According to our notation, the letter p is reserved for representing the period along an axis of movements. The classical distance between the parallel lines is represented by the letter T . The periods (p) are equal to the spaces between the lines (T), only when the lines are perpendicular to the movement axis (as in the case of Figure 2 with horizontal lines and a vertical movement axis). Our equations represent completely the inclined layer and moiré patterns and at the same time the formulas for computing moiré periods and optical speedups remain in their basic simple form (2.1), (2.2), and (2.3).

In this section we focus on linear movements. Equations binding inclination angles of layers and moiré patterns are based on p_r , p_b , and p_m , the periods of the revealing layer, base layer, and moiré lines respectively measured along the axis of movements.

For linear movements the p values represent distances along a straight axis. For rotational movements the p values represent the periods along circumference, i.e. the angular periods.

2.3.1. Shearing of simple parallel Moiré patterns

The superimposition of two layers with identically inclined lines forms moiré lines inclined at the same angle. Figure 3 (a) is obtained from Figure 1 with a vertical shearing. In Figure 3 (a) the layer lines and the moiré lines are inclined by 10 degrees. Inclination is not a rotation. During the inclination the distance between the layer lines along the vertical axis is conserved (p), but the true distance T between the lines (along an axis perpendicular to these lines) changes. The vertical periods p_b and p_r , and the distances T_b and T_r are indicated on the diagram of an example shown in Figure 5 (a).

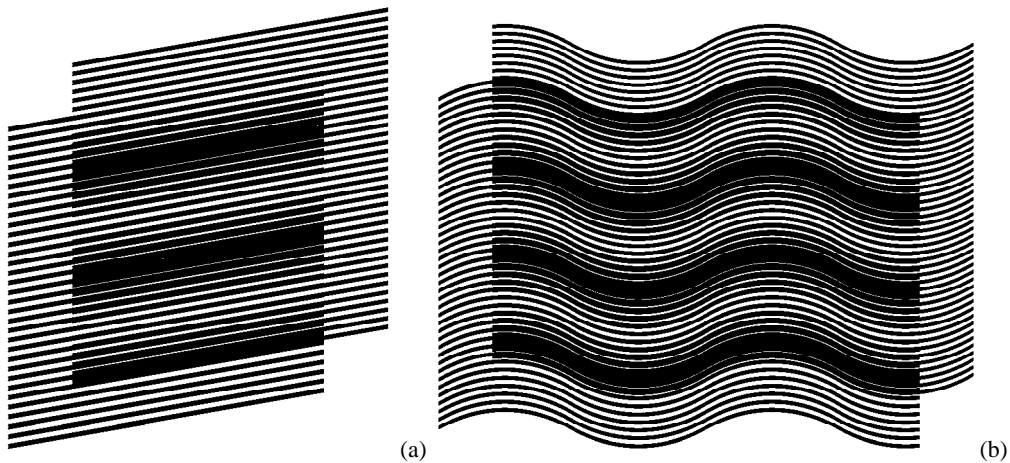


Figure 3. (a) Superposition of layers consisting of inclined parallel lines where the lines of the base and revealing layers are inclined at the same angle [eps], [png]; (b) Two layers consisting of curves with identical inclination patterns, and the superposition image of these layers [eps], [png]

The inclination degree of layer lines may change along the horizontal axis forming curves. The superposition of two layers with identical inclination pattern forms moiré curves with the same inclination pattern. In Figure 3 (b) the inclination degree of layer lines gradually changes according the following sequence of degrees (+30, -30, +30, -30, +30), meaning that the curve is divided along the horizontal axis into four equal intervals and in each such interval the curve's inclination degree linearly changes from one degree to the next according to the sequence of five degrees. Layer periods p_b and p_r represent the distances between the curves along the vertical axis, i.e. that of the movement. In Figure 3 (a) and (b), the ratio p_b / p_r is equal to 12/11. Figure 3 (b) can be obtained from Figure 1 by interpolating the image along the horizontal axis into vertical bands and by applying a corresponding vertical shearing and shifting to each of these bands. Equation (2.1) is valid for computing the spacing p_m between the moiré curves along the vertical axis and equation (2.3) for computing the optical speedup ratio when the revealing layer moves along the vertical axis.

2.3.2. Computing Moiré lines' inclination as a function of the inclination of layers' lines

More interesting is the case when the inclination degrees of layer lines are not the same for the base and revealing layers. Figure 4 shows four superposition images where the inclination degree of base layer lines is the same for all images (10 degrees), but the inclination degrees of the revealing layer lines are different and are equal to 7, 9, 11, and 13 degrees for images (a), (b), (c), and (d) respectively. The periods of layers along the vertical axis p_b and p_r (the p_b / p_r ratio being equal to 12/11) are the same for all images. Correspondingly, the period p_m computed with formula (2.1) is also the same for all images.

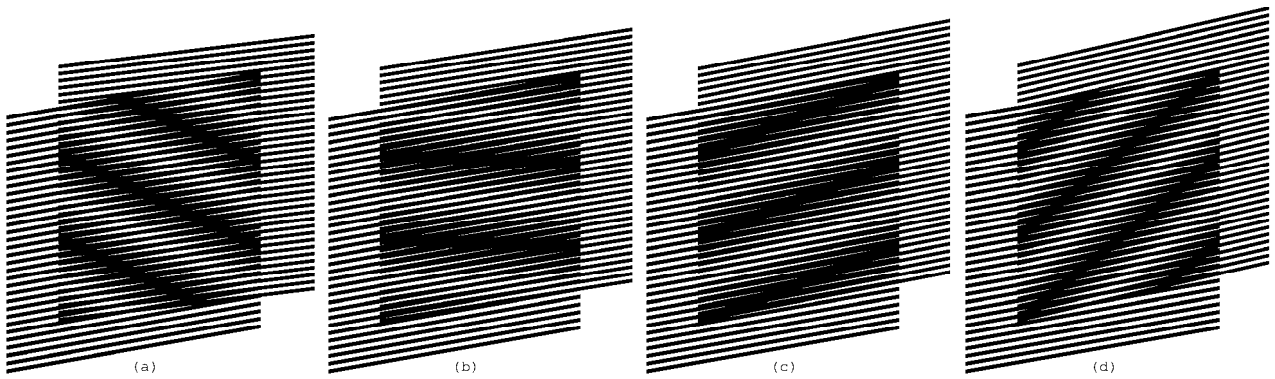


Figure 4. Superposition of layers consisting of inclined parallel lines, where the base layer lines' inclination is 10 degrees and the revealing layer lines' inclination is 7, 9, 11, and 13 degrees [eps (a)], [png (a)], [eps (b)], [png (b)], [eps (c)], [png (c)], [eps (d)], [png (d)]; GIF animation [ps], [gif], [tif]

Our web site shows a GIF animation [gif] of the superposition image of Figure 4 where the revealing layer's inclination oscillates between 5 and 15 degrees [Gabrielyan07b].

Figure 5 (a) helps to compute the inclination degree of moiré optical lines as a function of the inclination of the revealing and the base layer lines. We draw the layer lines schematically without showing their true thicknesses. The bold lines of the diagram inclined by α_b degrees are the base layer lines. The bold lines inclined by α_r degrees are the revealing layer lines. The base layer lines are vertically spaced by a distance equal to p_b , and the revealing layer lines are vertically spaced by a distance equal to p_r . The distance T_b between the base layer lines and the distance T_r between the revealing layer lines are the parameters used in the common formulas, well known in the literature. The parameters T_b and T_r are not used for the development of our equations. The intersections of the lines of the base and the revealing layers (marked in the figure by two arrows) lie on a central axis of a light moiré band that corresponds in Figure 4 to the light area between two parallel dark moiré lines. The dashed line passing through the intersection points

of Figure 5 (a) is the axis of the light moiré band. The inclination degree of moiré lines is therefore the inclination α_m of the dashed line.

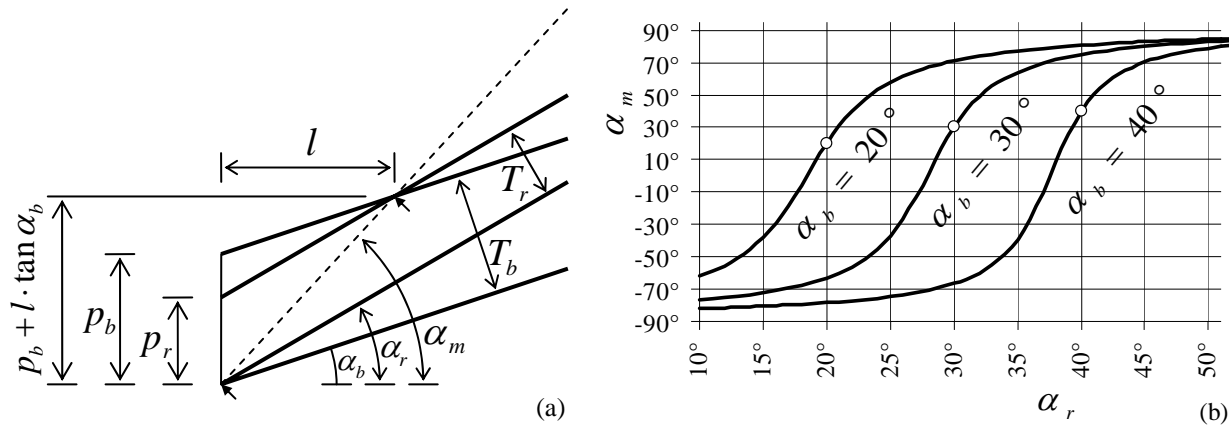


Figure 5. **(a)** Computing the inclination angle of moiré lines as a function of inclination angles of the base layer and revealing layer lines; **(b)** Moiré lines inclination as a function of the revealing layer lines inclination for the base layer lines inclination equal to 20, 30, and 40 degrees [xls]

From Figure 5 (a) we deduce the following two equations:

$$\begin{cases} \tan \alpha_m = \frac{p_b + l \cdot \tan \alpha_b}{l} \\ \tan \alpha_r = \frac{p_b - p_r + l \cdot \tan \alpha_b}{l} \end{cases} \quad (2.4)$$

From these equations we deduce the equation for computing the inclination of moiré lines as a function of the inclinations of the base layer and the revealing layer lines:

$$\tan \alpha_m = \frac{p_b \cdot \tan \alpha_r - p_r \cdot \tan \alpha_b}{p_b - p_r} \quad (2.5)$$

For a base layer period equal to 12 units, and a revealing layer period equal to 11 units, the curves of Figure 5 (b) represents the moiré line inclination degree as a function of the revealing layer line inclination. The base layer inclinations for the three curves (from left to right) are equal to 20°, 30°, and 40° degrees respectively. The circle marks correspond to the points where both layers' lines inclinations are equal and the moiré lines inclination also become the same.

2.3.3. Deducing the known formulas from our equations

The periods T_b , T_r , and T_m (see Figure 5 (a)) that are used in the commonly known formulas of the literature are deduced from periods p_b , p_r and p_m as follows:

$$T_b = p_b \cdot \cos \alpha_b \quad T_r = p_r \cdot \cos \alpha_r \quad T_m = p_m \cdot \cos \alpha_m \quad (2.6)$$

From here, using our equation (2.5) we deduce the well known formula for the angle of moiré lines [Amidor00a]:

$$\alpha_m = \arctan\left(\frac{T_b \cdot \sin \alpha_r - T_r \cdot \sin \alpha_b}{T_b \cdot \cos \alpha_r - T_r \cdot \cos \alpha_b}\right) \quad (2.7)$$

Recall from trigonometry the following simple formulas:

$$\cos \alpha = \frac{1}{\sqrt{1 + \tan^2 \alpha}} \quad (2.8)$$

$$\cos(\alpha_1 - \alpha_2) = \cos \alpha_1 \cdot \cos \alpha_2 + \sin \alpha_1 \cdot \sin \alpha_2$$

From equations (2.7) and (2.8) we have:

$$\cos \alpha_m = \frac{T_b \cdot \cos \alpha_r - T_r \cdot \cos \alpha_b}{\sqrt{T_b^2 + T_r^2 - 2 \cdot T_b \cdot T_r \cdot \cos(\alpha_r - \alpha_b)}} \quad (2.9)$$

From equations (2.1) and (2.6) we have:

$$T_m = \frac{T_b \cdot T_r}{T_b \cdot \cos \alpha_r - T_r \cdot \cos \alpha_b} \cdot \cos \alpha_m \quad (2.10)$$

From equations (2.9) and (2.10) we deduce the second well known formula in the literature, the formula for the period T_m of moiré lines:

$$T_m = \frac{T_b \cdot T_r}{\sqrt{T_b^2 + T_r^2 - 2 \cdot T_b \cdot T_r \cdot \cos(\alpha_r - \alpha_b)}} \quad (2.11)$$

Recall from trigonometry that:

$$\sin \frac{\alpha}{2} = \sqrt{\frac{1 - \cos \alpha}{2}} \quad (2.12)$$

In the particular case when $T_b = T_r$, taking in account equation (2.12), equation (2.11) is further reduced into well known formula:

$$T_m = \frac{T}{2 \cdot \sin\left(\frac{\alpha_r - \alpha_b}{2}\right)} \quad (2.13)$$

Still for the case when $T_b = T_r$, we can temporarily assume that all angles are relative to the base layer lines and rewrite equation (2.7) as follows:

$$\alpha'_m = \arctan\left(\frac{\sin \alpha'_r}{\cos \alpha'_r - 1}\right) \quad (2.14)$$

Recall from trigonometry that:

$$\tan \frac{\alpha}{2} = \frac{1 - \cos \alpha}{\sin \alpha} \quad (2.15)$$

$$\tan(90^\circ + \alpha) = -\frac{1}{\tan \alpha}$$

Therefore from equations (2.14) and (2.15):

$$\alpha'_m = 90^\circ + \frac{\alpha'_r}{2} \quad (2.16)$$

Now for the general case when the revealing layer lines do not represent the angle zero:

$$\alpha_m = \alpha_b + 90^\circ + \frac{\alpha_r - \alpha_b}{2} \quad (2.17)$$

We obtain the well known formula [[Amidoror00a](#)]:

$$\alpha_m = 90^\circ + \frac{\alpha_r + \alpha_b}{2} \quad (2.18)$$

Equations (2.7) and (2.11) are the general case formulas known in the literature, and equations (2.13) and (2.18) are the formulas for rotated identical patterns (i.e. the case when $T_b = T_r$) [[Amidoror00a](#)], [[Nishijima64a](#)], [[Oster63a](#)], [[Morse61a](#)].

Assuming in equation (2.7) that $\alpha_b = 0$, we have:

$$\alpha_m = \arctan \left(\frac{\sin \alpha_r}{\cos \alpha_r - \frac{T_r}{T_b}} \right) \quad (2.19)$$

Only for the case when $T_b = T_r$ the rotation of moiré lines is linear with respect to the rotation of the revealing layer (see equation (2.18)). Comparison of equation (2.19) and its respective graph (see [[Gabrielyan07a](#)]) with our equation (2.5) and its respective graph (see Figure 5 (b)) shows a significant difference in the binding of angles for sheared (i.e. inclined) and rotated layer patterns.

2.3.4. The revealing lines inclination as a function of the superposition image's lines inclination

From equation (2.5) we can deduce the equation for computing the revealing layer line inclination α_r for a given base layer line inclination α_b , and a desired moiré line inclination α_m :

$$\tan \alpha_r = \frac{P_r}{P_b} \cdot \tan \alpha_b + \left(1 - \frac{P_r}{P_b} \right) \cdot \tan \alpha_m \quad (2.20)$$

The increment of the tangent of the revealing lines' angle ($\tan(\alpha_r) - \tan(\alpha_b)$) relatively to the tangent of the base layer lines' angle can be expressed, as follows:

$$\tan \alpha_r - \tan \alpha_b = \left(1 - \frac{P_r}{P_b} \right) \cdot (\tan \alpha_m - \tan \alpha_b) \quad (2.21)$$

According to equation (2.3), $1 - \frac{P_r}{P_b}$ is the inverse of the optical acceleration factor, and therefore equation (2.21) can be rewritten as follows:

$$\frac{\tan \alpha_r - \tan \alpha_b}{\tan \alpha_m - \tan \alpha_b} = \frac{v_r}{v_m} \quad (2.22)$$

Equation (2.22) shows that relative to the tangent of the base layer lines' angle, the increment of the tangent of the revealing layer lines' angle needs to be smaller than the increment of the tangent of the moiré lines' angle, by the same factor as the optical speedup.

For any given base layer line inclination, equation (2.20) permits us to obtain a desired moiré line inclination by properly choosing the revealing layer inclination. In Figure 3 (b) we showed an example, where the curves of layers follow an identical inclination pattern forming a superposition image with the same inclination pattern. The inclination degrees of the layers' and moiré lines change along the horizontal axis according the following sequence of alternating degree values (+30, -30, +30, -30, +30). In Figure 6 (a) we obtained the same superposition pattern as in Figure 3 (b), but the base layer consists of straight lines inclined by -10 degrees. The corresponding revealing pattern is computed by interpolating the curves into connected straight lines, where for each position along the horizontal axis, the revealing line's inclination angle is computed as a function of $\alpha_b = -10^\circ$ and α_m , according to equation (2.20).

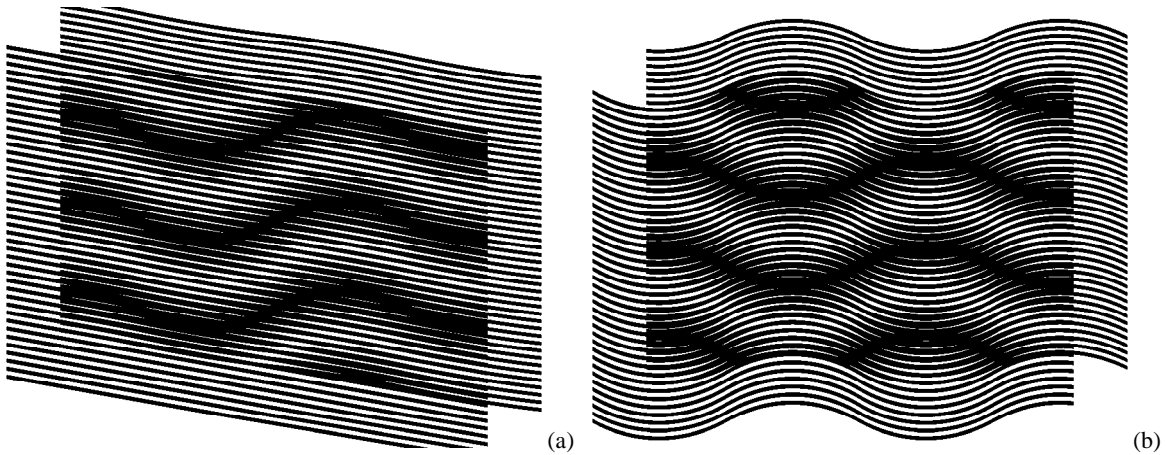


Figure 6. (a) The base layer with inclined straight lines and the revealing layer computed so as to form the desired superposition image [eps], [png]; (b) Inversed inclination patterns of moiré and base layer curves [eps], [png]; GIF animation [ps], [tif], [gif]

The same superposition pattern as in Figure 3 (b) and Figure 6 (a) is obtained in Figure 6 (b). Note that in Figure 6 (b) the desired inclination pattern (+30, -30, +30, -30, +30) is obtained using a base layer with a completely inverted inclination pattern (-30, +30, -30, +30, -30).

Figure 6 (a) and (b) demonstrate what is already expressed by equation (2.22): the difference between the inclination patterns of the revealing layer and the base layer are several times smaller than the difference between the inclination patterns of moiré lines and the base layer lines.

Our web page contains a GIF animation [gif] for modifying pairs of base and revealing layers constantly forming the same superposition image of Figure 3 (b), Figure 6 (a), and Figure 6 (b) i.e. the moiré inclination pattern (+30, -30, +30, -30, +30) [Gabrielyan07b]. In the animation, the base layer inclination pattern gradually changes and the revealing layer inclination pattern correspondingly adapts such that the superposition image's inclination pattern remains the same.

3. SUPERPOSITION OF PERIODIC CIRCULAR PATTERNS

3.1. Superposition of circular periodic patterns with radial lines

Similarly to layer and moiré patterns comprising parallel lines (see Figure 1), concentric superposition of dense periodic layer patterns comprising radial lines forms magnified periodic moiré patterns also with sparse radial lines.

Figure 7 is the counterpart of Figure 1, where the horizontal axis is replaced by the radius and the vertical axis by the angle. Full circumferences of layer patterns are equally divided by integer numbers of radial lines. The number of radial lines of the base layer is denoted as n_b and the number of radial lines of the revealing layer is denoted as n_r .

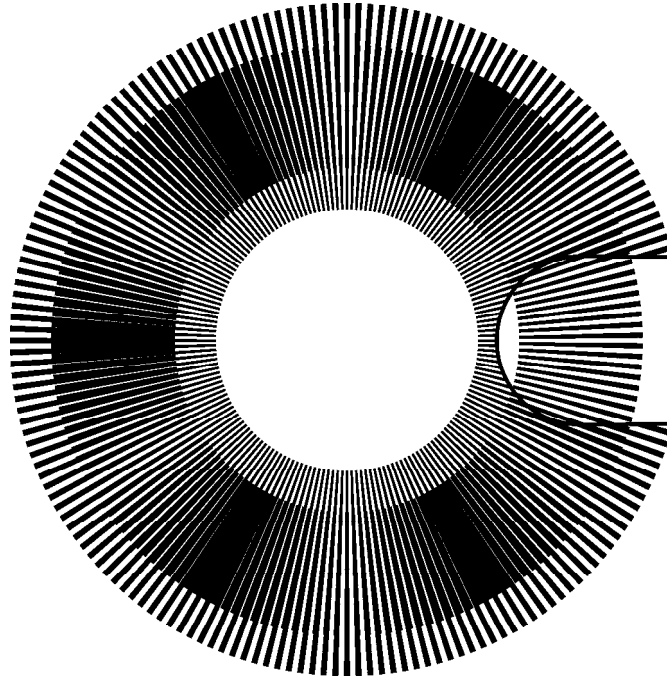


Figure 7. Superposition of two layers with regularly spaced radial segments (a portion of the revealing layer is cut out to show a part of the base layer in the background) [\[eps\]](#), [\[png\]](#); GIF animation [\[ps\]](#), [\[tif\]](#), [\[gif\]](#)

The periods p_b and p_r denote the angles between the central radial axes of adjacent lines. Therefore:

$$p_b = \frac{360^\circ}{n_b}, \quad p_r = \frac{360^\circ}{n_r} \quad (3.1)$$

According to equations (3.1), equation (2.1) can be rewritten as follows:

$$p_m = \frac{360^\circ}{n_r - n_b} \quad (3.2)$$

Therefore the number of moiré radial lines n_m corresponds to the difference between the numbers of layer lines:

$$n_m = |n_r - n_b| \quad (3.3)$$

If in the layer patterns, the full circumferences are divided by integer numbers of layer lines, the circumference of the superposition image is also divided by an integer number of more lines.

The optical speedup factor of equation (2.3) can be rewritten by replacing the periods p_r and p_b by their expressions from equations (3.1):

$$\frac{v_m}{v_r} = \frac{n_r}{n_r - n_b} \quad (3.4)$$

The values v_r and v_m represent the angular speeds. The negative speedup signifies a rotation of the superposition image in a direction inverse to the rotation of the revealing layer. Considering (3.3), the absolute value of the optical speedup factor is:

$$\left| \frac{v_m}{v_r} \right| = \frac{n_r}{n_m} \quad (3.5)$$

Radial lines have constant angular thickness, giving them the forms of segments, thick at their outer ends and thin at their inner ends. The values of p_m , n_m , and v_m/v_r do not depend on the angular thickness of radial lines. In our examples the angular thicknesses of layer lines are equal to the layer's half-period, i.e. the thickness of the base layer lines is equal to $p_b/2$ and the thickness of the revealing layer lines is $p_r/2$.

In Figure 7, the number of radial lines of the revealing layer is equal to 180, and the number of radial lines of the base layer is 174. Therefore, according to equations (3.4) and (3.3), the optical speedup is equal to 30, confirmed by the two images (a) and (b) of Figure 8, and the number of moiré lines is equal to 6, confirmed by the image of Figure 7.

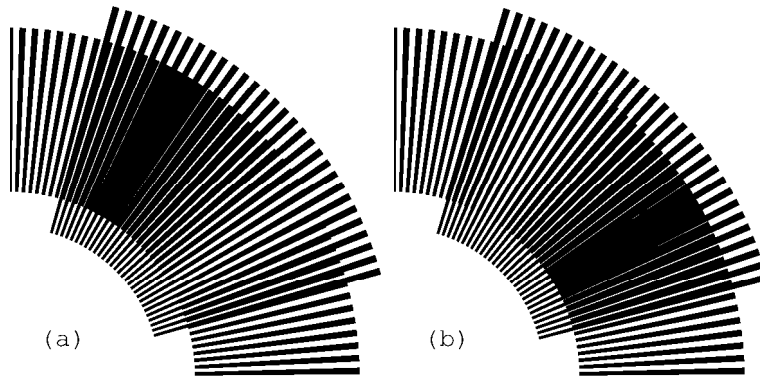


Figure 8. Rotation of the revealing layer by 1 degree in the clockwise direction rotates the optical image by 30 degrees in the same direction [[eps \(a\)](#)], [[png \(a\)](#)], [[eps \(b\)](#)], [[png \(b\)](#)]

A GIF animation [[gif](#)] of the superposition image of Figure 7, where the revealing layer slowly rotates in the clockwise direction is available on our web site [[Gabrielyan07b](#)].

3.2. Superposition of circular patterns with radial curves

In circular periodic patterns curved radial lines can be constructed using the same sequences of inclination degrees as used in section 2.3 for curves of Figure 3 (b). The inclination angle at any point of the radial curve corresponds to the angle between the curve and the axis of the radius passing through the current point. Thus inclination angle 0 corresponds to straight radial lines as in Figure 7. With the present notion of inclination angles for α_b , α_r , and α_m , equations (2.5) and (2.20) are applicable for circular patterns without modifications.

Curves can be constructed incrementally with a constant radial increment equal to Δr . Figure 9 shows a segment of a curve, marked by a thick line, which has an inclination angle equal to α .

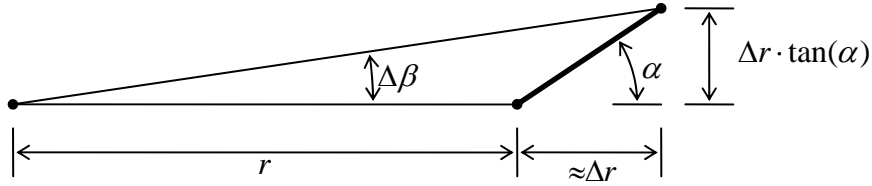


Figure 9. Constructing a curve in a polar coordinate system with a desired inclination

While constructing the curve, the current angular increment $\Delta\beta$ must be computed so as to respect the inclination angle α :

$$\Delta\beta \approx \arctan\left(\frac{\Delta r \cdot \tan(\alpha)}{r + \Delta r}\right) \approx \frac{180^\circ}{\pi \cdot r} \cdot \Delta r \cdot \tan(\alpha) \quad (3.6)$$

Figure 10 shows a superposition of layers with curved radial lines. The inclination of curves of both layers follows an identical pattern corresponding to the following sequence of degrees (+30, -30, +30, -30, +30). Layer curves are iteratively constructed with increment pairs $(\Delta r, \Delta\beta)$ computed according to equation (3.6). Since the inclination patterns of both layers of Figure 10 are identical, the moiré curves also follow the same pattern.

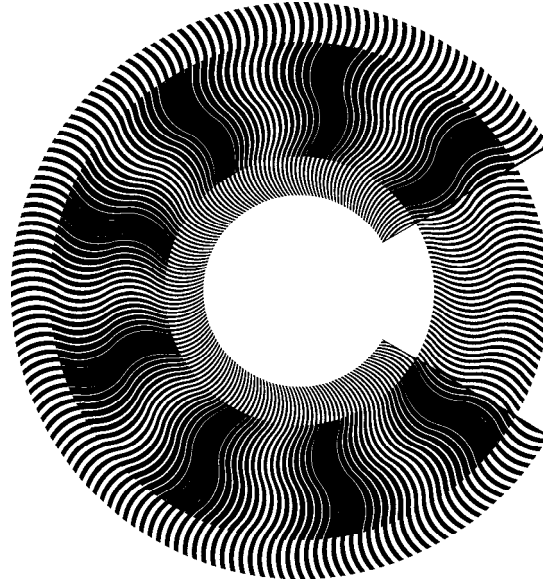


Figure 10. Superposition of layers in a polar coordinate system with identical inclination patterns of curves corresponding to (+30, -30, +30, -30, +30); a portion of the revealing layer is cut away exposing the base layer in the background [eps], [png], multi-page [tif], [gif]

Our web page [Gabrielyan07b] shows the superposition image of Figure 10 in motion [gif] when the revealing layer slowly rotates in clockwise direction.

Similarly to examples of Figure 3 (b), Figure 6 (a), and Figure 6 (b), where the same moiré pattern is obtained by superposing different pairs of layer patterns, the circular moiré pattern of Figure 10 can be analogously obtained by superposing other pairs of circular layer patterns. Taking into account equations (3.1), equations (2.5) and (2.20) can be rewritten as follows:

$$\tan \alpha_m = \frac{n_r \cdot \tan \alpha_r - n_b \cdot \tan \alpha_b}{n_r - n_b} \quad (3.7)$$

$$\tan \alpha_r = \frac{n_b}{n_r} \cdot \tan \alpha_b + \left(1 - \frac{n_b}{n_r}\right) \cdot \tan \alpha_m \quad (3.8)$$

Taking into account equation (3.4), equation (3.8) can be also rewritten as follows:

$$\tan \alpha_r = \left(1 - \frac{v_r}{v_m}\right) \cdot \tan \alpha_b + \frac{v_r}{v_m} \cdot \tan \alpha_m \quad (3.9)$$

For producing the superposition image of Figure 10, thanks to equations (3.8) and (3.9), other pairs of layer patterns can be created as shown in Figure 11. In the first image (a) of Figure 11, the base layer lines are straight. In the second image (b), the base layer lines inclination pattern is reversed with respect to the moiré lines.

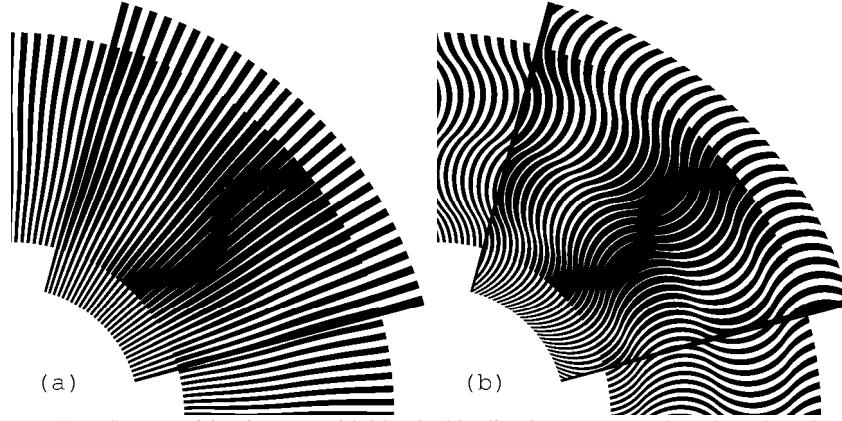


Figure 11. Superposition images with identical inclination pattern (+45, -45, +45, -45, +45) of moiré curves, where in one case the base layer comprise straight radial segments, and in the second case the base layer comprise curves which are the mirrored counterparts of the resulting moiré curves [eps (a)], [png (a)], [eps (b)], [png (b)]; Animation [eps], [tif], [gif]

Our web page [Gabrielyan07b] contains an animation [gif], where the moiré curves of the superposition image are always the same, but the inclination pattern of the base layer curves gradually alternates between the following two mirror patterns (+45, -45, +45, -45, +45), and (-45, +45, -45, +45, -45). For each instance of the animation, the revealing layer lines are computed according to equation (3.8) in order to constantly maintain the same moiré pattern.

Equations (3.4) and (3.3) remain valid for patterns with curved radial lines. In Figure 10 there are 180 curves in the revealing layer and 171 curves in the base layer. Therefore optical speedup factor according to equation (3.4) is equal to 20, and the number of moiré curves according to equation (3.3) is equal to 9, as seen in the superposition image of Figure 10.

4. LAYER PATTERNS WITH SPIRALS IN A SINGLE RING

One can form a radial moiré fringe with a period equal to 360° . In the superposition image of such pattern we will see only one moiré fringe. This fringe will not have sharp contours and will appear large and blurred. The radial moiré fringe can be formed by layer patterns with radial lines or rather radial sectors. For small speed ratios, fine granularity of layer patterns with radial lines cannot be maintained. As the speed ratio decreases, the superposition image becomes coarse and the moiré shape becomes visually not identifiable. The fine granularity can be maintained by using spiral shaped lines in layer patterns. The layer patterns with spirals can be computed such that the moiré fringe is kept

radially oriented. By reducing the spiral elevation rate in both layers, sufficiently fine layer patterns can be obtained. However, strongly inclined spirals resulting to fine patterns make the superposition moiré images less tolerant to mechanical inaccuracies such as surface deformations of layers or disparities in concentric superposition of layers.

In Figure 12 we show that a design extension of simple spiral patterns with a single moiré fringe may result to a useful application.

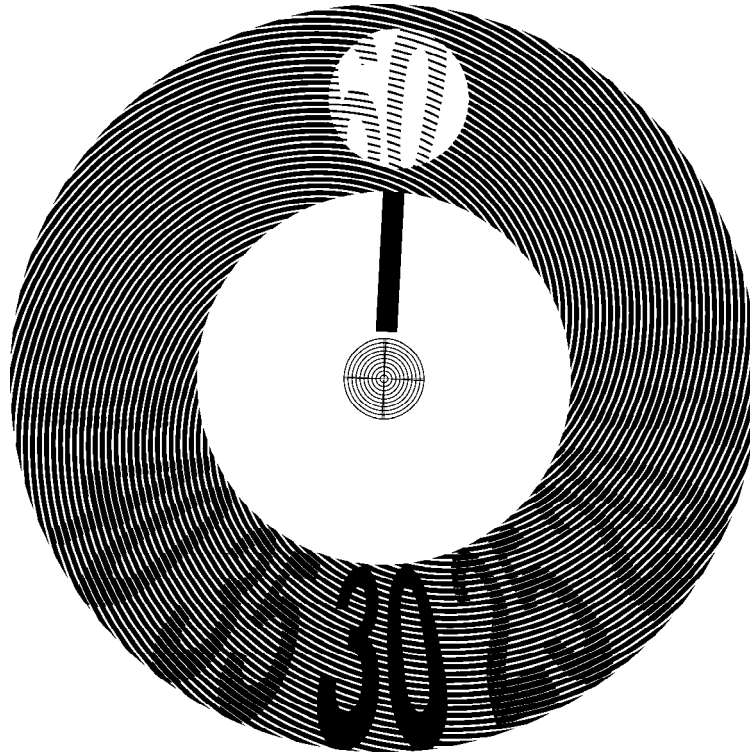


Figure 12. Mono-ring moiré with a speed ratio equal to 60; a single moiré fringe; the spirals of one of the layers are clipped within contours of labels [\[eps\]](#), [\[png\]](#), [\[gif\]](#), [\[tif\]](#)

The example is obtained by taking a simple spiral pattern of a base layer and by cleaning in such pattern all areas lying outside the contours of twelve labels. A part of the revealing layer is cut-away exposing the base layer. In such a way, instead of revealing a large and blurred moiré fringe, our superposition pattern reveals more attractive image consisting of labels within the concerned area. The area rotates at a 60 times faster speed than the mechanical rotation speed of the revealing layer. The spirals of two layers are computed so as to produce a moiré fringe with radial orientation.

Our web page [\[Gabrielyan07b\]](#) contains the animation [\[gif\]](#) of the superposition image shown in Figure 12, for a slow rotation of the revealing layer by 6° contraclockwise.

5. MULTI-RING MOIRÉ

In this section we present our multi-ring circular patterns. The superimposition of our multi-ring layer patterns forms a complex moiré image, but at one position a continuous shape is outlined. When rotating the revealing layer, the optical shape rotates without deformations at a k times faster speed.

5.1. Multi-ring patterns with constant ring widths

Refer to equation (3.4) for circular patterns. An optical rotation k times faster than the rotation of the revealing layer can be obtained if:

$$\begin{aligned}n_r &= k \cdot i \\n_b &= (k - 1) \cdot i\end{aligned}\tag{5.1}$$

where $i \in \{1, 2, \dots\}$, $\frac{v_m}{v_r} = k$

According to equation (3.3) the number n_m of moiré spots in a circular pattern for different values of i is simply equal to the value of i :

$$\begin{aligned}n_m &= n_r - n_b \\n_m &= i\end{aligned}\tag{5.2}$$

Therefore, the same moiré speedup factor k can be obtained with different pairs of revealing and base layer patterns corresponding to different numbers n_m of moiré bands. We can construct several nested concentric circular patterns for the same value of k and for different values of i .

For example, Figure 13 shows four nested adjacent rings, where the index i increments from 1 to 4 when counting from the inner ring toward the outer ring. The number of dark moiré radial lines of individual rings changes from 1 to 4 according to equation (5.2). The acceleration factor k is equal to 60 for all rings. Therefore the revealing layer of the most inner ring has 60 radial lines and the corresponding base layer has 59 lines. Correspondingly the layers of the most outer ring have 240 and 236 radial lines. In Figure 13 a part of the revealing layer is cut out, exposing the base layer. All rings are constructed such that the lines of the revealing and base layers perfectly overlap at the angle zero. Therefore a light moiré radial band appears at the angle zero of each individual rings.

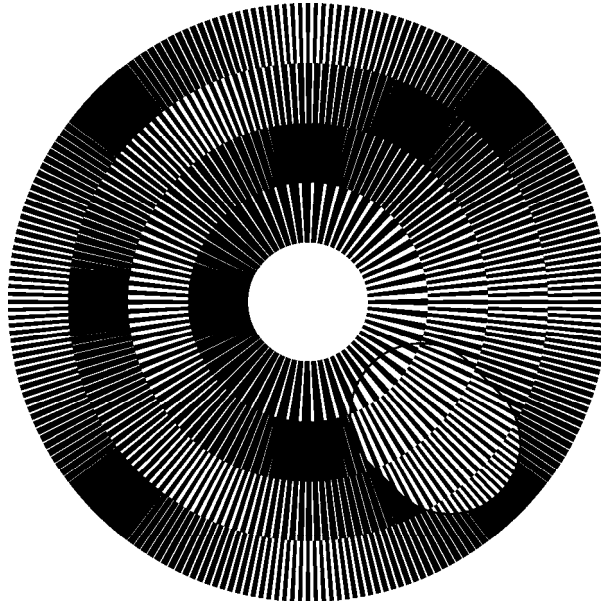


Figure 13. Four nested rings whose layer lines overlap at angle zero [\[eps\]](#), [\[png\]](#)

For the inner ring, the dark moiré band is located at 180 degrees from angle zero. The first dark moiré band of the second ring is located at 90 degrees. The first dark moiré band of the third ring is located at 60 degrees and for the most outer ring at 45 degrees.

The patterns of the base and revealing layers of each ring can be printed so as a dark moiré band appears at the angle zero. For this purpose, both layer patterns of each ring must be rotated by a degree γ :

$$\gamma = -\frac{360^\circ}{2 \cdot n_m} \quad (5.3)$$

Figure 14 corresponds to the superimposition image of Figure 13, but the individual ring patterns are rotated according to equation (5.3) such that dark moiré bands appear at the angle zero in all rings. The black moiré bands of all adjacent rings became horizontally aligned forming a joint radial shape.

Once the rings are adjusted according to equation (5.3), we consider that the base layer patterns of all rings form a single joint base layer (e.g. printed on an opaque paper), and the revealing layer patterns of all rings form a joint revealing layer (e.g. printed on a transparency). A part of the revealing layer is cut away exposing the base layer.

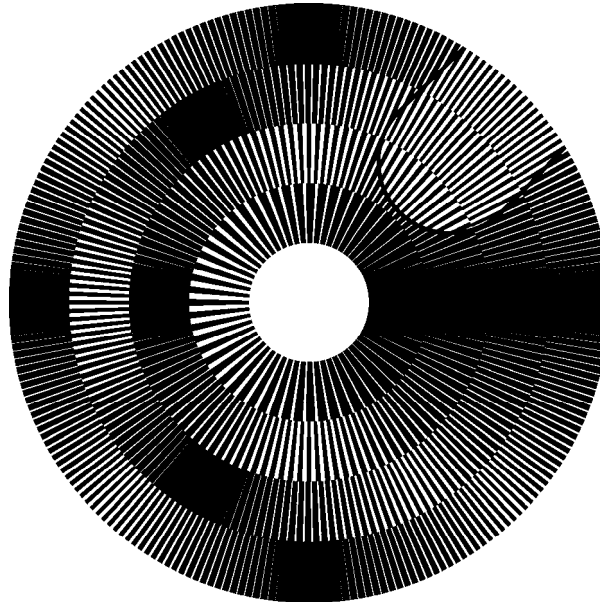


Figure 14. Four nested rings with an acceleration factor equal to 60 for all four rings [\[eps\]](#), [\[png\]](#)

According to equation (5.1), rotation of the revealing layers at a given angular speed must rotate the superimposition image at another angular speed which is identical for all rings. Therefore the radial moiré band traversing all rings will remain aligned all the time during the rotation. Rotation of the revealing layer rotates the optical image at a k times faster speed.

The acceleration factor k of the superimposition image of Figure 14 is equal to 60. Therefore the rotation of the revealing layer by -1 degree rotates the optical image by -60 degrees (compare the image of Figure 14 with the first image of Figure 15). Rotation of the revealing layer by -2 degree rotates the optical image by -120 degrees (compare the image of Figure 14 with the second image of Figure 15). The negative rotation angles correspond to the rotation in clockwise direction. The negligible rotations of the revealing layer in Figure 14 and Figure 15 can be noticed by observing the cut out region of the revealing layer.

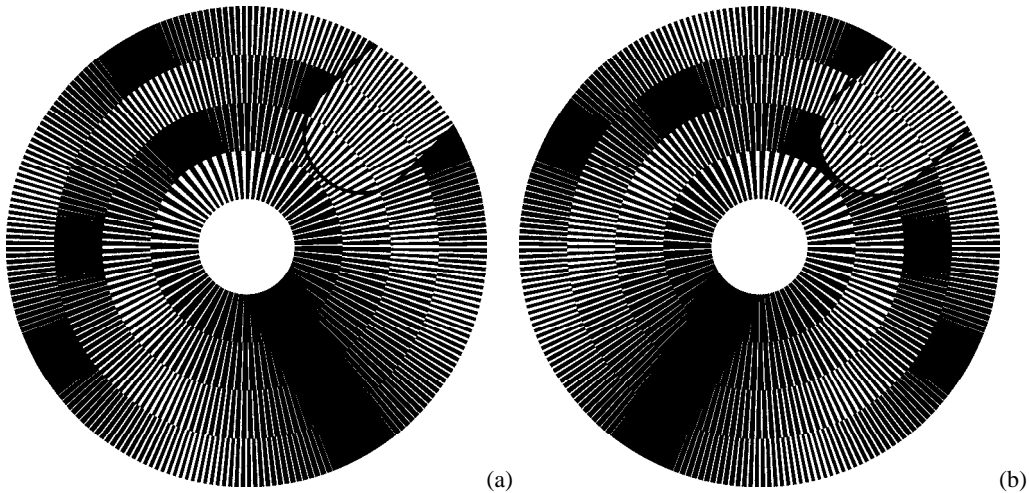


Figure 15. Multi-ring moiré for different angles of rotation of the revealing layer [[eps \(a\)](#)], [[png \(a\)](#)], [[eps \(b\)](#)], [[png \(b\)](#)]; Animation [[ps](#)], [[tif](#)], [[gif](#)]

In our web site [[Gabrielyan07b](#)] we present a GIF file [[gif](#)] which demonstrates the superposition image shown in Figure 14 and Figure 15 during a rotation of the revealing layer that slowly turns by 6 degree in clockwise direction. During this time the superimposition image makes a full rotation of 360 degree also in clockwise direction.

5.2. Multi-ring patterns with variable ring widths and a non-incrementing number of moiré bands

The widths of the rings of the multi-ring patterns must not be obligatorily the same. The number n_m of the ring's moiré bands also must not necessarily increment with the ring number. Figure 16 shows a superimposition image with 12 rings, where at the beginning the number of moiré bands increments, but after reaching a maximal limit at a ring j_0 , the number of moiré bands starts decrementing. The maximal number of moiré bands is set to 10. Therefore the number of moiré bands n_m follows the following sequence (1, 2, 3, ... 8, 9, **10**, 9, 8). The ring widths are not constant and are computed so as the largest ring is the ring j_0 , at which n_m has its maximal value. The adjacent rings gradually decrease their widths as we move away from the largest ring.

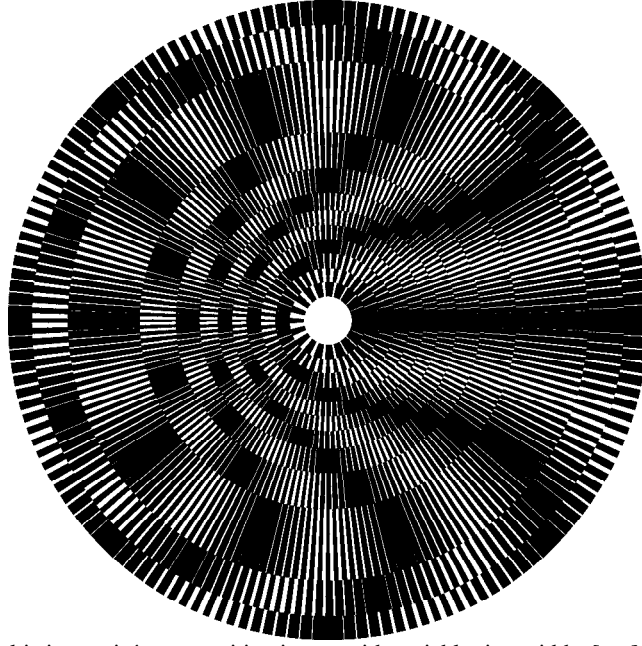


Figure 16. Multi-ring moiré superposition image with variable ring widths [eps], [png]

The width w_j of the j -th ring can be computed by equation (5.4), where j is the sequential number of the ring, j_0 is the number of the widest ring, w_{\min} is the minimal ring width, and w_{\max} is the maximal ring width.

$$w_j = \frac{w_{\max}}{1 + \min\left(|j - j_0|, \frac{w_{\max}}{w_{\min}} - 1\right)} \quad (5.4)$$

6. MULTI-RING MOIRÉ WITH INCLINED LINE PATTERNS

6.1. Straight radial Moiré lines with curved layer lines

Recall that for measuring the line inclination in circular patterns we use the angle α between the line and the radial axis as shown in Figure 9. In Figure 16, inclination of moiré lines of the superposition image is equal to 0 degree for all rings. In section 3.2 we show that the desired degree of moiré inclination can be obtained by different pairs of base and revealing layer patterns.

It is sufficient to choose for every ring an inclination pattern of the base layer and then, the corresponding inclination pattern of the revealing layer can be computed thanks to equation (3.8) or (3.9). Taking into account that in multi-ring patterns the speedup factor k used in equations (5.1) is the same for all rings, equation (3.9) can be rewritten as follows:

$$\tan \alpha_r = \left(1 - \frac{1}{k}\right) \cdot \tan \alpha_b + \frac{1}{k} \cdot \tan \alpha_m \quad (6.1)$$

For a particular case, when $\alpha_m = 0$, i.e. when we desire straight radial moiré lines, equation (6.1) is further reduced to:

$$\tan \alpha_r = \left(1 - \frac{1}{k}\right) \cdot \tan \alpha_b \quad (6.2)$$

For any inclination of the base layer pattern, the revealing layer pattern can be computed according to equation (6.2) to ensure straight radial moiré lines. Figure 17 shows a superposition image with straight moiré lines, similarly to Figure 14. In contrast to Figure 14 the base layer lines are not straight. The overall inclination pattern of the entire base layer across all rings follows the following sequence of inclination degrees $(-30^\circ, +30^\circ, -30^\circ, +30^\circ)$.

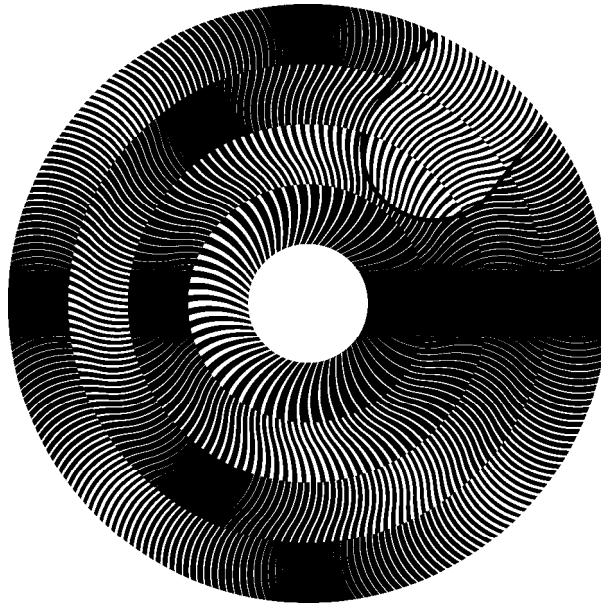


Figure 17. Multi-ring moiré superposition image, where the inclination of moiré lines is of 9 degree and the inclination of the base layer lines follows the following inclination pattern $(-30, +30, -30, +30)$ [\[eps\]](#), [\[png\]](#), [\[ps\]](#), [\[gif\]](#)

The GIF animation [\[gif\]](#) of the pattern of Figure 17 is provided on our web site [\[Gabrielyan07b\]](#).

Figure 18 is the counterpart of Figure 16. In both figures the pattern of variable ring widths is computed by equation (5.4). In contrast to Figure 16 the base layer lines of Figure 18 are not straight. The overall inclination pattern of the base layer across all rings follows the following sequence of inclination degrees $(+30^\circ, -30^\circ, +30^\circ)$. The revealing layer line inclinations are computed according to equation (6.2) so as the superposition image forms the same straight moiré line shape as in Figure 16.

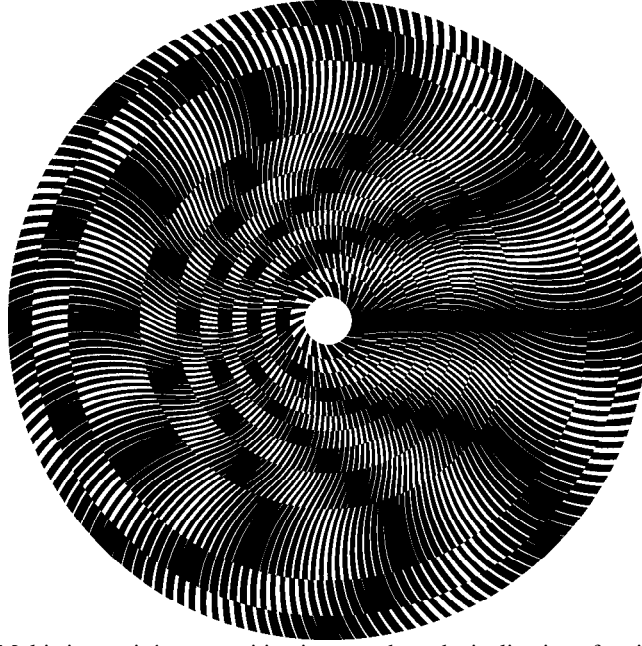


Figure 18. Multi-ring moiré superposition image, where the inclination of moiré lines is of 0 degree and the inclination of the base layer lines follows the following inclination pattern (+30, -30, +30) [eps], [png]

Inclined and curved layer patterns can be used for maintaining a uniform fine granularity across the surface of the disk. When the density of radial layer lines is sparse, the granularity can be refined by increasing the inclination degree.

6.2. Curved Moiré lines in Multi-ring patterns

In Figure 14, Figure 16, Figure 17, and Figure 18 we assemble the base layer and revealing layer patterns from rings rotated according equation (5.3), such that in the superposition image, the moiré fringes are aligned along the angle zero.

Equation (5.3) does not hold for cases when the moiré fringes themselves are curved. In this section we introduce multi-ring patterns with curved moiré shapes.

The curved moiré fringes of individual rings must join into a continuous moiré shape across the multi-ring superposition pattern. The angle γ of equation (5.3) for every successive ring must be additionally adjusted by the angular shift gained by the moiré curve while traversing the preceding rings.

Let $\alpha_m(r)$ be the inclination of the moiré line as a function of the radius r . Let r_j and r_{j+1} be the inner and outer radiuses of the j -th ring. According to equation (3.6) the angular gain β_j of the moiré curve within the j -th ring is expressed as follows:

$$\beta_j = \int_{r_j}^{r_{j+1}} \frac{180}{\pi} \cdot \frac{\tan \alpha_m(r)}{r} \cdot dr \quad (6.3)$$

The aggregate angular gain $\beta_{1,j}$ up to the j -th ring is computed as follows:

$$\beta_{1,j} = \frac{180}{\pi} \cdot \sum_{q=1}^j \int_{r_q}^{r_{q+1}} \frac{\tan \alpha_m(r)}{r} \cdot dr \quad (6.4)$$

Equation (5.3) must be rewritten so as to consider also the adjustment brought by equation (6.4):

$$\gamma = \frac{180}{\pi} \cdot \sum_{q=1}^j \int_{r_q}^{r_{q+1}} \frac{\tan \alpha_m(r)}{r} \cdot dr - \frac{360}{2 \cdot n_m} \quad (6.5)$$

With the angular adjustments of ring patterns computed by equation (6.5), we can create a continuous moiré curve jointly lying across all rings of the pattern. Figure 19 shows a serpentine shaped moiré curve. There are 14 rings of equal width. The acceleration factor k is equal to 30. The number n_m of moiré spots increments starting from 1, for the inner ring, through 14 for the most outer ring. The base layer line inclination pattern corresponds to the following sequence of angles $(-80, +10, -10, +10, -30)$. The revealing layer line inclination pattern is computed according to equation (6.1) so as to ensure the following moiré inclination pattern $(+30, -30, +30, -30, +30)$. A small part of the revealing layer is cut away exposing the uncovered part of the base layer pattern.

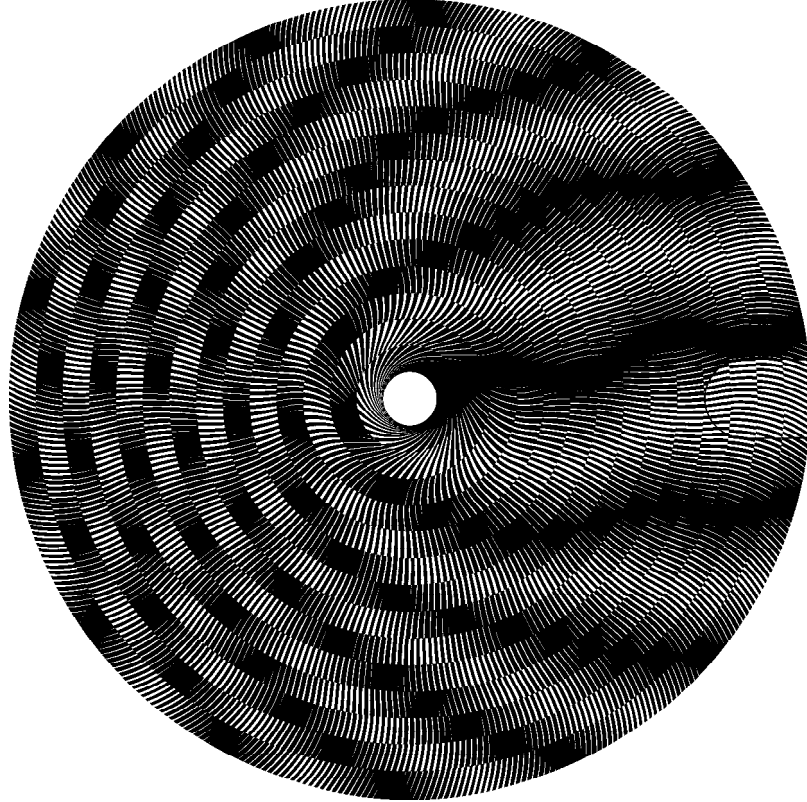


Figure 19. Multi-ring moiré with a continuous serpentine-shaped moiré curve [eps], [png]

Figure 20 shows a serpentine-shaped moiré curve in a multi-ring moiré with a variable ring width pattern of Figure 16 described by equation (5.4). There are 14 rings; the acceleration factor is equal to 30. The base layer inclination pattern is $(-80, 5, 0, -5, -80)$, the moiré inclination pattern is $(30, -30, 30, -30, 30)$; the revealing layer inclination pattern is computed with equation (6.1).

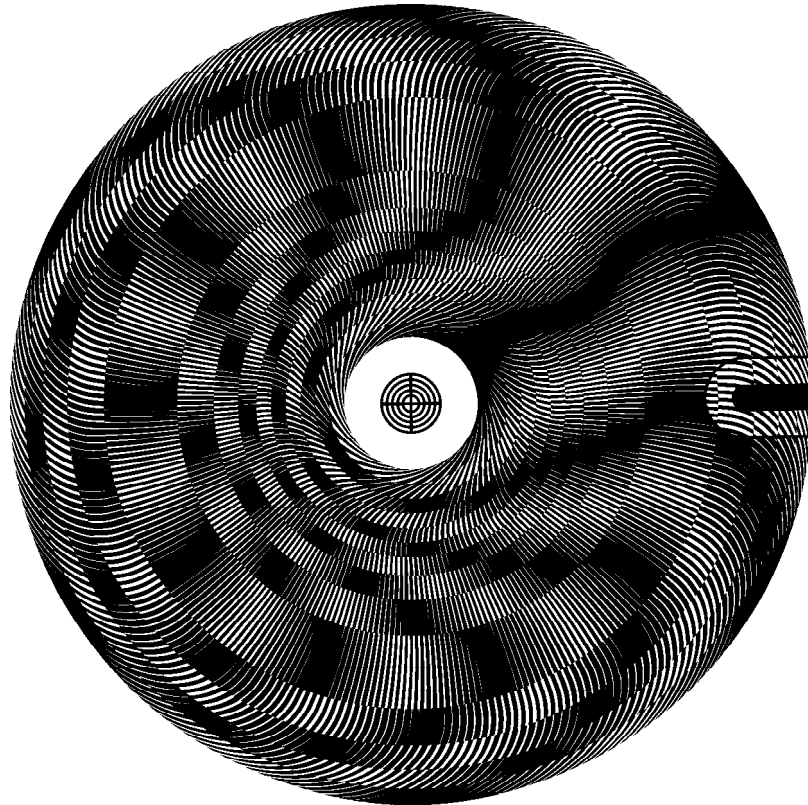


Figure 20. Multi-ring pattern with serpentine-shaped moiré curve and with variable ring width
[\[eps\]](#), [\[png\]](#), multi-page [\[tif\]](#), [\[ps\]](#), [\[gif\]](#)

Our web site [\[Gabrielyan07b\]](#) contains a GIF animation [\[gif\]](#) of Figure 20.

7. CONCLUSIONS

Many basic measurement instruments comprising a mechanical scale and a mechanical pointer have often their developed versions with a supplementary sub-graduated scale and an auxiliary mechanical pointer which moves faster and aims at the precision increase. A mechanical gearing system is used for a fast movement of the auxiliary pointer synchronously with the main pointer.

We developed layer patterns forming optical moiré shapes suitable for the auxiliary fast indicator. Mechanical transmission systems are not required. Moiré shapes can be obtained by superposition of transparent layers carrying correlated opaque patterns. The following points are important: (a) the moiré shapes must be sharp, (b) highly periodic moiré shapes cannot be used for indication, (c) the periodicity of moiré shapes must be very long corresponding to the visible window of the superposition image, such that one and only one shape is visible at a time, e.g. in circular moiré the period of moiré shapes must be equal to 360 degree; (d) the optical speedup of the mechanical movement must be linear; (e) the said above must be valid for the full range of mechanical movements of the main pointer putting into motion the revealing layer, e.g. in circular patterns for the full range of 360 degree rotation of the revealing layer.

Sharp moiré shapes are easily formed in well known simple periodic moiré patterns; however their periodicity is very high and cannot be used for indication. Long periods, such as 360 degrees for circular moiré, can be obtained with simple moiré patterns; however the moiré shape becomes blurred and not acceptable for indication. The known random line moiré offers completely aperiodic shapes without the required long periodicity. Additionally, their shapes are noisy compared with their periodic counterparts.

We introduced multi-stripe and multi-ring moiré patterns offering very long periods suitable for measurement purposes and forming moiré shapes as sharp as in highly periodical patterns.

We developed equations for producing straight and curved auxiliary moiré pointers across multi-ring moiré patterns. We can obtain a moiré shape of any desired curve that can be represented by a continuous function. Our equations help to obtain the desired moiré shape for different base layer patterns by finding the matching revealing layer pattern.

In our model, the choice of the shape of the moiré fringe has no impact on the dynamic properties of the auxiliary moiré pointer. We preserve the speedup formulas in their simplest form (2.1), (2.2), and (2.3) for linear movements and (3.2), (3.3), (3.5), and (3.4) for rotations regardless the inclination patterns of layers and moiré shapes.

8. REFERENCES

- [[Amidror00a](#)] Isaac Amidror, *The Theory of the Moiré Phenomenon*, Kluwer Academic Publisher, 2000 [[CH](#)], [[US](#)]
- [[Amidror03a](#)] Isaac Amidror, "Glass patterns in the superposition of random line gratings", *Journal of Optics A: Pure and Applied Optics*, pp. 205-215, 28 March 2003 [[CH](#)], [[US](#)]
- [[Amidror03b](#)] Isaac Amidror, "Glass patterns as moiré effects: new surprising results", *Optics Letters* (Optical Society of America), Vol. 28, Issue 1, pp. 7-9, 1 January 2003 [[CH](#)], [[US](#)], [[epfl](#)]
- [[Gabrielyan07a](#)] Emin Gabrielyan, "The basics of line moiré patterns and optical speedup", arXiv, 9 pages, 8 March 2007, <http://www.arxiv.org/abs/physics/0703098>, paper [[CH](#)], [[US](#)], web [[CH](#)], [[US](#)]
- [[Gabrielyan07b](#)] Emin Gabrielyan, "Fast optical Indicator created with multi-ring moiré Patterns", Switzernet research reports, 4 August 2007, <http://switzernet.com/people/emin-gabrielyan/070804-moire-rings>
- [[Glass69a](#)] Leon Glass, "Moiré Effect from Random Dots", *Nature* 223, pp. 578-580, 1969 [[CH](#)], [[US](#)], [[Nature](#)]
- [[Glass73a](#)] Leon Glass and Rafael Pérez, "Perception of Random Dot Interference Patterns", *Nature* 246, pp. 360-362, 7 December 1973, [[CH](#)], [[US](#)], [[ca](#)]
- [[Hutley99](#)] M.C. Hutley and R.F. Stevens, "Optical inspection of arrays and periodic structures using moire magnification", *IEE Colloquium: Microengineering in Optics and Optoelectronics*, No. 187, p. 8, 16 November 1999
- [[Kamal98](#)] Hala Kamal, Reinhard Völkel, and Javier Alda, "Properties of moiré magnifiers", *Optical Engineering* 37 (11), pp. 3007-3014, November 1998 [[CH](#)], [[US](#)]
- [[Morse61a](#)] Stanley Morse, August J. Durelli, and Cesar A. Sciammarella, "Geometry of moiré fringes in strain analysis", *American Society of Civil Engineers*, Vol. 126, Part I, pp. 250-271, 1961 [[CH](#)], [[US](#)]
- [[Nishijima64a](#)] Y. Nishijima and G. Oster, "Moiré patterns: their application to refractive index and refractive index gradient measurements", *Journal of the Optical Society of America*, Vol. 54, No. 1, pp. 1-5, January 1964 [[CH](#)], [[US](#)]
- [[Oster63a](#)] G. Oster and Y. Nishijima, "Moiré patterns", *Scientific American*, Vol. 208, pp. 54-63, May 1963
- [[Sciammarella62a](#)] C. A. Sciammarella and A. J. Durelli, "Moiré fringes as a means of analyzing strains", *American Society of Civil Engineers*, Vol. 127, Part I, pp. 582-587, 1962 [[CH](#)], [[US](#)]